International Journal of Mass Spectrometry 330–332 (2012) 134–143

Contents lists available at SciVerse ScienceDirect

International Journal of Mass Spectrometry

journal homepage: www.elsevier.com/locate/ijms

IRMPD and DFT study of the loss of water from protonated 2-hydroxynicotinic acid

Michael Van Stipdonk[a,*], Michael Kullman[b], Giel Berden[c], Jos Oomens[c,d]

[a] Department of Chemistry, Lawrence University, Appleton, WI, USA
[b] Department of Chemistry, Wichita State University, Wichita, KS, USA
[c] FOM Institute for Plasma Physics Rijnhuizen, Nieuwegein, The Netherlands
[d] University of Amsterdam, Science Park 904, 1098X Amsterdam, The Netherlands

ARTICLE INFO

Article history:
Received 25 April 2012
Received in revised form 25 June 2012
Accepted 29 June 2012
Available online 7 July 2012

This paper is dedicated to Peter B. Armentrout, an inspiring physical chemist and colleague, on the occasion of his 60th birthday.

Keywords:
IRMPD
Ion structure
DFT
Fragmentation mechanism
Reaction dynamics

ABSTRACT

Collision-induced dissociation (CID) of protonated 2-hydroxynicotinic acid (2-OHNic) generates a dominant product ion through loss of 18 mass units, presumably the elimination of water. Subsequent isolation and storage of this product ion in the gas-phase environment of an ion trap mass spectrometer, without imposed collisional activation, shows that the species undergoes addition reactions to furnish new products that are higher in mass by 18 and 32 units. Density functional theory (DFT) calculations suggest that an acylium ion (i.e., loss of H_2O from the acid group) is energetically more favored than is a species generated by elimination of H_2O from the hydroxypyridine ring. Formation of the acylium product is confirmed by comparing the infrared multiple photon dissociation (IRMPD) spectrum to theoretical spectra from (DFT) harmonic calculations for several possible isomers. A thorough DFT study of the reaction dynamics suggests that the acylium ion is generated from the global minimum for the protonated precursor along a pathway that involves proton transfer from the hydroxypyridine ring and elimination of —OH from the acid group.

1. Introduction

Proton transfer is an important part of the fragmentation mechanisms of protonated peptides using low-energy collision-induced dissociation (CID). Indeed, development of the *mobile proton* model [1,2] of peptide fragmentation, and related amide bond cleavage pathways [3–10], has been focused primarily on proton mobilization. The *pathways in competition* (PIC) fragmentation model [11] uses the mobile proton model as a foundation for understanding, but takes into account the structures and reactivity of key reactive configurations and primary fragments as well as transition states and their energies.

As part of an on-going effort by our group to understand the mechanism(s) of peptide fragmentation, we have investigated CID of protonated peptides with N-terminal nicotinic acid residues [12,13]. In the experiments to date, the pyridine ring of nicotinic acid was used to fix the charge (protonation) site to determine whether sequestering "mobile" protons influences peptide fragmentation. In one study [12], b_2^+ was found to be the dominant product ion generated from protonated nicotinic acid-glycine-glycine methyl ester, arising by cleavage of the amide bond between glycine residues. Infrared multiple photon dissociation (IRMPD) spectroscopy and density functional theory (DFT) calculations unambiguously showed that the protonation site for the intact peptide was the pyridine ring of the nicotinic acid residue rather than amide carbonyl oxygen atoms. More importantly, the IRMPD spectrum revealed that the b_2 fragment ion has a conventional oxazolone structure also protonated at the N-atom of the pyridine ring. The fact that both ions are protonated at the pyridine ring was consistent with a proposed mechanism in which the added proton was "fixed" at the pyridine ring and amide position protons are mobilized and transferred to generate b_2^+.

In an earlier study [13], we investigated transfer of H atoms by McLafferty rearrangement using two model peptide systems, protonated nicotinyl-glycine-*tert*-butyl ester and the cationic betaine-glycine-*tert*-butyl ester, using IRMPD spectroscopy. McLafferty rearrangement was used to generate the free-acid forms of the respective model peptides through transfer of an H atom and elimination of butene. The resulting peptide ions were then subjected to

* Corresponding author at: Department of Chemistry, Lawrence University, 711 E. Boldt Way, Appleton, WI 54911, USA. Tel.: +1 920 832 6533.
E-mail address: michael.j.vanstipdonk@lawrence.edu (M. Van Stipdonk).

1387-3806/$ – see front matter © 2012 Elsevier B.V. All rights reserved.
http://dx.doi.org/10.1016/j.ijms.2012.06.026

wavelength-selective IRMPD to measure their vibrational spectra. Comparison of the IRMPD spectra to those predicted by DFT allowed definitive assignment of absorption bands corresponding to the free-acid carbonyl, amide I and amide II stretches, and enabled assignment of ion structure. For the nicotinyl-glycine system, the best match between IRMPD and theoretical spectra, both in terms of the respective absorption frequencies and relative intensities, was obtained for a conformational isomer that is protonated at the pyridine ring N atom, and includes an intra-molecular hydrogen bonding interaction between the amide position H atom and the C-terminal carbonyl O atom.

Support for the intra-molecular transfer of the H atom by McLafferty rearrangement was produced using the model peptide *tert*-butyl esters incubated in a mixture of D_2O and CH_3OD to induce H/D exchange [13]. For the deuterium-exchanged peptide ester, CID and McLafferty rearrangement produces a heterogeneous isotopically labeled peptide ion containing two D atoms and one H atom at exchangeable sites. Comparison of the IRMPD results to theoretical spectra for different isotope labeled isomers clearly showed that the H atom is situated at the C-terminal acid group and migration to amide positions is minimal on the time scale of the experiment.

Our attention in the present study was directed to the fragmentation of protonated 2-hydroxynicotinic acid (2-OHNic), which generates a dominant product ion through the elimination of water. Loss of H_2O can occur from the acid group, or from the hydroxypyridine ring: in both cases the fragmentation route would require intramolecular proton transfer.

Subsequent isolation and storage of the product in the gas-phase environment of an ion trap mass spectrometer, without imposed collisional activation, shows that the species undergoes addition reactions to furnish new products that are 18 and 32 mass units higher. These reactions are consistent with "reforming" of the acid, or generation of a methyl ester, by reaction of water or methanol with an acylium ion. The process is therefore reminiscent of the last step in formation of carboxylic acids from olefins, a process for which acylium ions are thought to be intermediates [14,15]. Acylium ions are also thought to be important intermediates in, for example, the solvolysis of benzoyl halides [16], alkyl thiobenzoates [17] and amides [18], in Friedel–Crafts acylation [19], and in the Schmidt reaction [20] and Hayashi rearrangement [21,22].

To shed more light on the mechanism(s) by which the dehydration of 2-OHNic occurs, most probable conformations for the protonated precursor ion, and various possible product ions generated by CID through loss of H_2O, were investigated using DFT. The structures of gas-phase, protonated 2-OHNic and the dehydrated product were then determined using IRMPD spectroscopy. Lastly, the reaction dynamics for three potential pathways were investigated using DFT, and the lowest energy pathway is one that involves formation of an acylium by proton transfer and elimination of —OH from the acid group. The experiments illuminate facets of an interesting gas-phase reaction, contribute to the understanding of proton transfer in dissociation pathways and further illustrate the reactivity of acylium ions.

2. Experimental methods

2.1. Materials and sample preparation

2-Hydroxynicotinic acid (2-OHNic) was purchased from ThermoFisher Scientific (St. Louis, MO, USA) and used as received. Solutions for ESI MS and IRMPD spectroscopy were prepared by dissolving the appropriate amount of solid material in a 1:1 (v:v) mixture of HPLC grade MeOH (Aldrich Chemical, St. Louis, MO) and deionized H_2O to produce final concentrations of 10^{-5} to 10^{-4} M. Because of the labile nature of 2-OHNic, no formic or acetic acid was added to the solution to enhance ionization efficiency. Under the conditions employed in this study, acceptable $(M+H)^+$ ion intensities were produced for both ion-trap CID and FT-ICR IRMPD investigations. Investigation of the fragmentation of deuterium labeled 2-OHNic was carried out after incubating the species in a mixture of D_2O/CD_3OD (Aldrich Chemical, St. Louis, MO).

2.2. Ion trap mass spectrometry experiments

CID spectra were collected using a Finnigan LCQ-Deca ion-trap mass spectrometer (ThermoFinnigan, San Jose, CA, USA). Each of the peptide solutions were infused into the ESI-MS instrument using the incorporated syringe pump at a flow rate of 5 μl/min. The atmospheric pressure ionization stack settings for the LCQ (lens voltages, quadrupole and octopole voltage offsets, etc.) were optimized for maximum $(M+H)^+$ transmission to the ion trap mass analyzer by using the auto-tune routine within the LCQ Tune program. Helium was used as the bath/buffer gas to improve trapping efficiency and as the collision gas for CID experiments.

The $(M+H)^+$ ions were isolated for the initial CID stage (MS/MS) using an isolation width of 1.2–1.8 mass to charge (m/z) units. Product ions selected for subsequent CID (MS^3 experiments) were isolated using widths of 1.2–1.5 m/z units. For each stage, the width was chosen empirically to produce the best compromise between high precursor ion intensity and ability to isolate a single isotopic peak. The (mass) normalized collision energy (NCE, as defined by ThermoFinnigan) was set between 20 and 25%, which corresponds the application of roughly 0.55–0.68 V tickle voltage to the end cap electrodes with the current instrument calibration. To probe gas-phase ion molecule reactivity, specific product ions are isolated and stored in the ion trap, without imposed collisional activation. The activation *Q*, which defines the frequency of the applied R.F. potential, was set at 0.30. In all cases, the activation time employed was 30 ms. Spectra displayed represent the accumulation and averaging of at least 30 isolation, dissociation and ejection/detection steps.

2.3. ESI FT-ICR mass spectrometry

Previously established methods were used for generation of ions and the subsequent collection of IRMPD spectra [23–30]. Briefly, ESI was performed using a Micromass Z-Spray source. Ions were injected into a home-built Fourier transform ion cyclotron resonance (FT-ICR) mass spectrometer described in detail elsewhere [28]. Instrument operating parameters, such as desolvation temperature, cone voltage, and ion accumulation and transfer optics voltages, were optimized to maximize formation of $(M+H)^+$ ions, or b_2 ions generated by in-source CID, and transfer of the species to the ICR cell. Dry nitrogen (~80 °C) was used to assist in the desolvation process. Ions were accumulated for the duration of the previous FT-ICR cycle (approximately 5 s) in an external hexapole and injected into the ICR cell via a quadrupole deflector and an octapole R.F. ion guide.

In the relatively high pressures in a quadrupole ion trap mass spectrometer, the "dehydrated" product undergoes fast addition reactions, as discussed later. Similar behavior is also observed if attempts to produce the dehydrated product in the electrospray ionization source region. For the IRMPD experiments, the dehydrated product ion was generated from the protonated 2-OHNic ion under high vacuum conditions (ca. 10^{-7} Torr) within the ICR cell by photodissociation using the output of a continuous wave 30 W CO_2 IR laser (2 s irradiation time). After formation, the dehydrated product showed no tendency to re-generate the carboxylic acid through addition of H_2O, consistent with the low pressure and lack of adventitious water in the ICR cell.

2.4. Infrared multiple photon dissociation (IRMPD)

Infrared spectra were recorded by measuring the photodissociation yield as a function of photon wavelength. Precursor ions were irradiated using 30 FELIX macropulses (35 mJ per macropulse, 5 μs pulse duration, 10 FWHM bandwidth ~0.5% of central λ). In the IRMPD process, a photon is absorbed when the laser frequency matches a vibrational mode of the gas-phase ion and its energy is subsequently distributed over all vibrational modes by intramolecular vibrational redistribution (IVR). The IVR process allows the energy of each photon to be dissipated before the ion absorbs another, which leads to promotion of ion internal energy toward the dissociation threshold via multiple photon absorption [29]. It is important to note that infrared spectra obtained using IRMPD are comparable to those collected using linear absorption techniques [30,31]. For the current experiments, the free electron laser wavelength was tuned between 5 and 7.2 μm in 0.025 μm increments. The intensity of product and un-dissociated precursor ions was measured using the excite/detect sequence of the FT-ICR-MS after each IRMPD step. The IRMPD yield was normalized to the total ion current, and linearly corrected for variations in laser power across the wavelength range scanned.

2.5. DFT geometry and frequency calculations

All DFT calculations were performed using the Gaussian 03 group of programs [32]. Full geometry optimizations for protonated 2-OHNic and various product ion structures were initiated using the hybrid B3LYP functional and the 6–31G(d) basis set on all atoms. Using the minima identified at this level of theory, relaxed scans were performed by rotating (through 360°) dihedral angles in 3° steps to continue the search for alternative structures. Minima identified for all four ions were then re-optimized using the same functional and the 6-311+G(d,p) and 6-311++G(3df,3p) basis sets. Vibrational spectra and (zero-point corrected) relative energies were computed at the B3LYP/6-311++G(3df,3p) level of theory. The vibrational frequencies are scaled by factors chosen empirically to facilitate comparison to the IRMPD spectra. For protonated 2-OHNic, the scaling factor of 0.98 used brought the acid C=O stretch for the spectrum predicted for the global minimum into agreement with the absorption in the IRMPD spectrum. For the dehydrated product, the scaling factor that provided the best comparison was 0.96. To compare theoretical to experimental IR spectra, the former are convoluted with a Lorentzian profile with 10 cm^{-1} width at half maximum.

Transition states along the potential energy surfaces for possible reaction pathways were determined using the QST2 and QST3 method. All transitions states were confirmed by the presence of a single imaginary frequency. Intrinsic reaction coordinates were performed where necessary to confirm that the identified transition states bridged the appropriate minima.

3. Results and discussion

3.1. CID of protonated 2-OHNic

The ESI mass spectrum of 2-OHNic in the range mass to charge ratio (*m*/*z*) 90–150 is shown in Fig. 1a. ESI of 2-OHNic in a 50/50 mix of H_2O and methanol primarily generates the protonated ion at *m*/*z* 140. A minor peak (<10% relative intensity) at *m*/*z* 122 was also observed using the experimental conditions employed. In the CID spectrum (MS/MS stage, Fig. 1b) collected from protonated 2-OHNic, the only product ion generated appears at *m*/*z* 122, a mass difference of 18 mass units (u) that is attributed to loss of H_2O. The neutral loss shifted to 20 mass units (u) when CID of the fully deuterium exchanged version of 2-OHNic was examined (data not shown), consistent with the proposed fragmentation channel.

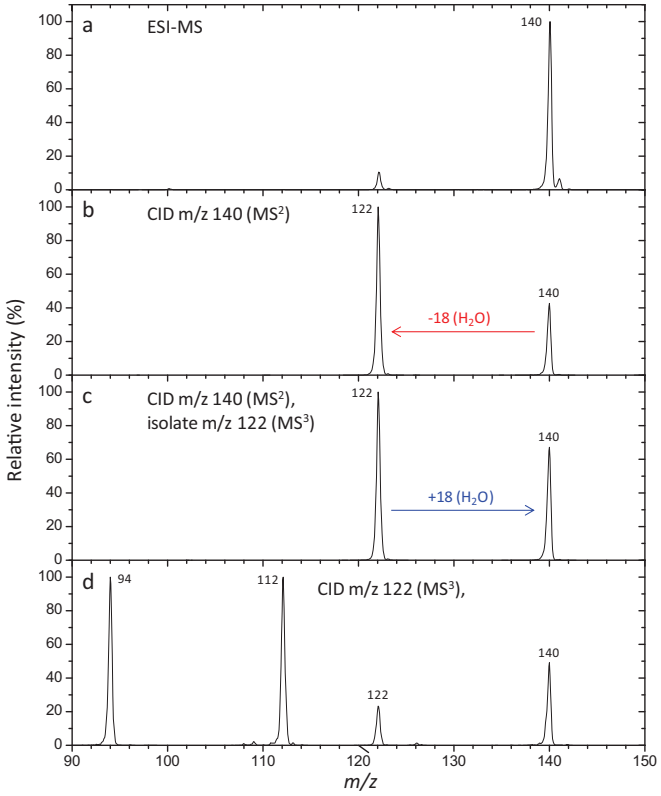

Fig. 1. Mass spectra derived from 2-hydroxynicotinic acid: (a) full mass spectrum, (b) CID of protonated 2-hydroxynicotinic acid (*m*/*z* 140), (c) isolation of *m*/*z* 122, without imposed collisional activation, after generation from protonated 2-hydroxynicotinic acid (MS^3 stage) and (d) CID (MS^3 stage) of *m*/*z* 122 product ion derived from protonated 2-hydroxynicotinic acid.

The relative intensities of the ions at *m*/*z* 122 and 140 in Fig. 1b remained similar even when the applied collision voltage was increased to 40–50% of the NCE, values that are much higher than those typically required to fragment small protonated species such as 2-OHNic. This observation suggested either that there were two or more species in the ion population with significantly different dissociation thresholds, or that the ion at *m*/*z* 140 is regenerated by ion-molecule reactions between the *m*/*z* 122 ion and adventitious water in the quadrupole ion trap. The proposed involvement of H_2O as a collision partner is plausible based on recent work demonstrating that CID within ion trap instruments involves a significant number of activating collisions between precursor ions and small molecules such as N_2 and H_2O present as contaminants within the He bath gas [33–36].

The ion at *m*/*z* 122 was isolated and stored in the ion trap, without imposed collision voltage, for 30 ms in an MS^3 experiment. The resulting product ion spectrum is shown in Fig. 1c. It is important to note that all species other than the ion at *m*/*z* 122 are resonantly ejected from the ion trap prior to the imposed isolation time of 30 ms. Additional product ions present in the spectrum are therefore the result of gas-phase ion-molecule reactions that occur within the environment of the ion trap. The spectrum displayed in Fig. 1c shows that the species at *m*/*z* 140 is formed from an ion-molecule reaction involving the ion at *m*/*z* 122. The appearance of the *m*/*z* 140 ion therefore suggests that the 2-OHNic species is regenerated, as a protonated ion, by the reaction of the *m*/*z* 122 ion with adventitious H_2O in the ion trap. The intensity of the *m*/*z* 140 ion increased with increasing imposed isolation time, consistent

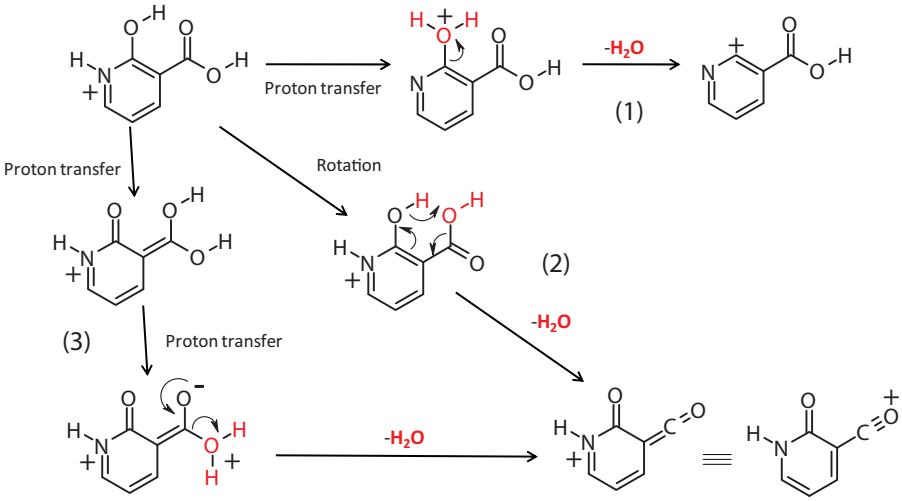

Scheme 1. Possible routes for elimination of H_2O during CID of protonated 2-hydroxynicotinic acid.

with the hypothesis that the species generated at the MS^3 stage is created by an ion-molecule reaction within the ion trap.

Similar experiments were performed using ESI spray solutions prepared using 2-OHNic dissolved in pure MeOH or ethanol (data not shown). After a period of 30 min with spray of the alcohol solutions (presumably allowing introduction of sufficient quantities of MeOH or EtOH into the ion trap to allow each to serve as neutral reagents in ion-molecule reactions), adducts to the *m*/*z* 122 ion at *m*/*z* 154 and 168, respectively, were observed. This suggests that reactions to produce the methyl and ethyl esters of 2-OHNic were generated in the gas-phase after the *m*/*z* 122 ions was generated by CID.

The ion-molecule reactivity of the *m*/*z* 122 fragment ion in these experiments is reminiscent of earlier work involving specific product ions generated by CID [37–39]. For example, Guan and Liesch [37] reported that product ions generated from a class of protonated pharmaceutical molecules participated in ion-molecule reactions with ESI solvent molecules (for example, water, acetonitrile and aliphatic alcohols) to form adducts. The reactive product ions were proposed to be acylium ions based on rational interpretation of the fragmentation of the precursor species. Later, Stein and coworkers [38] demonstrated that the intensities of product ions from protonated quinoline drug precursors were sensitive to a range of operating parameters during selected ion monitoring by tandem mass spectrometry. Apparent changes in ion intensity were ultimately traced to formation of adducts to specific (acylium type) ions by ion-molecule reactions. The work by Stein and coworkers was a follow-up to an earlier investigation of similar compounds by Kaufmann and coworkers [39].

In the present study, the apparent product ions generated by CID of the product ion at *m*/*z* 122 (MS^3 stage, Fig. 1d) initially derived from protonated 2-OHNic appeared at *m*/*z* 94 and 112. The *m*/*z* 94 ion corresponds to the elimination of 28 mass units, presumably CO, from the ion at *m*/*z* 122. The species at *m*/*z* 112 was identified as an ion generated by addition of H_2O to the *m*/*z* 94 product by isolating the latter, with storage without imposed collisional activation, in the ion trap for 30 ms.

Three plausible routes to elimination of H_2O from protonated 2-OHNic are shown in Scheme 1. Protonated 2-OHNic may either be in the 2-pyridone form with the added proton located at the O atom of the ring-carbonyl group, or adopt the tautomeric hydroxypyridine form with the proton instead added at the N-atom of the ring. Route 1 is initiated by tautomerization, with proton transfer from the N atom of the ring to create a hydroxypyridine-like structure with the added proton also located at the ring carbonyl O atom. Cleavage of the C—OH_2 bond results in elimination of H_2O. The product ion thus generated has a structure reminiscent of a nicotinic acid carbocation.

In route 2, rotation of the acid group is followed by proton transfer and elimination of H_2O through a 6-member ring transition state to furnish an acylium ion with a 2-pyridone like structure. The same product ion is generated through route 3, but by a process in which proton transfer from the protonated 2-pyridone ring to the carbonyl O atom of the acid group is followed by transfer to the —OH group. Elimination of H_2O then furnishes the acylium ion.

Of the proposed pathways, routes 2 and 3 are most consistent with the observed fragmentation of the *m*/*z* 122 product ion. Loss of CO from the acylium structure would furnish a 2-hydroxypyridine carbocation, or the keto tautomer. Fragmentation of the product ion generated by route 1 might instead be expected to involve elimination of CO_2 or CO_2H. Proton transfer steps in both routes 1 and 3 would appear to proceed through suprafacial 1–3 transition states that are (symmetry) forbidden, and thus likely to have relatively large (>150 kJ/mol) barriers.

3.2. Structures predicted by DFT

Possible structures for protonated 2-OHNic and the dehydrated product ion are shown in Figs. 2 and 3, respectively. Relative energies for the respective conformations, obtained from B3LYP/6-311+G(d,p) and B3LYP/6-311++G(3df,3p) calculations, are provided in Tables 1 and 2. For intact 2-OHNic, the majority of the minima identified correspond to structures with a 2-pyridone-type structure of the ring that differ in the position of the added proton. Two structures, **OHNic_p3** and **OHNic_p11**, are stable ion-molecule complexes composed of the acylium ion and H_2O. Of the respective minima, the lowest energy structure is **OHNic_p1**, for which the conformation identical to the one depicted as the starting species in Scheme 1. Structures in which the added proton is positioned on the acid group rather than on the 2-pyridone ring range from ~21 to 99 kJ/mol higher in energy. Similar species that are protonated at the acid group, but which adopt the hydropyridine conformation (**OHNic_p20** and **OHNic_p21**) are ~76 to 120 kJ/mol higher in energy.

The lowest energy structures predicted for the dehydrated product ions are acylium ions. Structure **OHNic_p4** is an acylium ion with 2-pyridone configuration of the ring and is lowest in energy. The acylium ion with the tautomeric hydroxypyridine configuration of

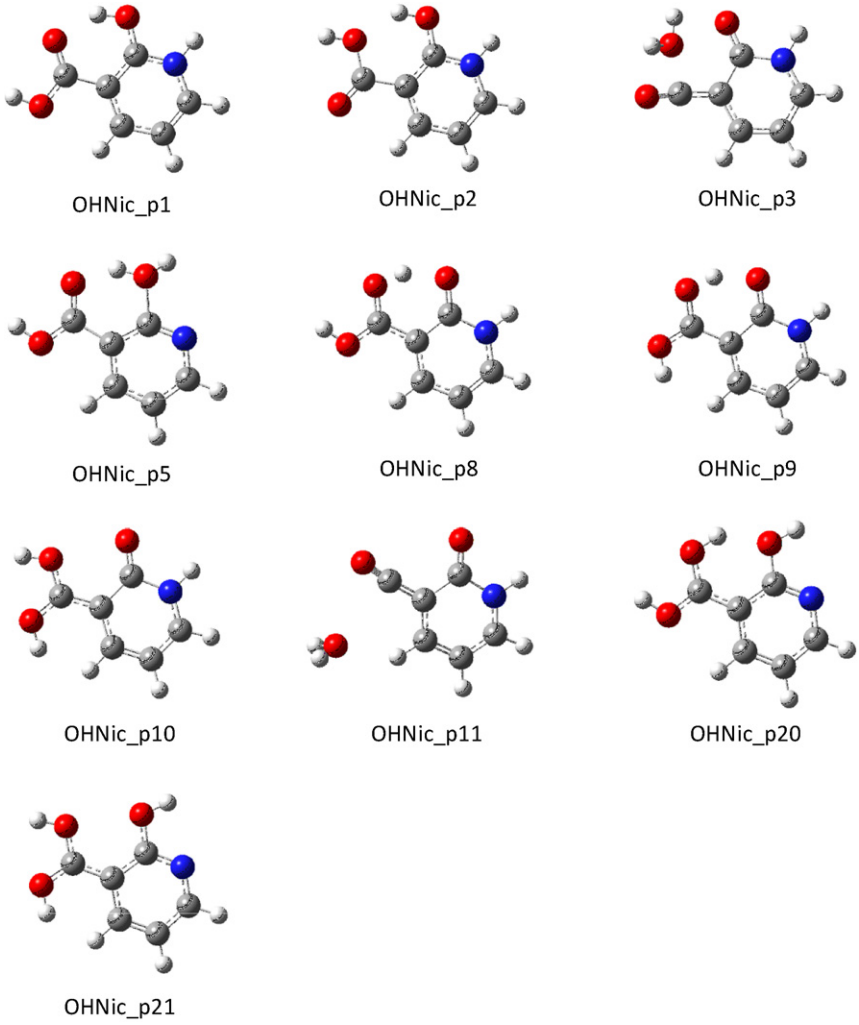

Fig. 2. Structures predicted for protonated 2-hydroxynicotinic acid (B3LYP/6-311+G(d,p) level of theory).

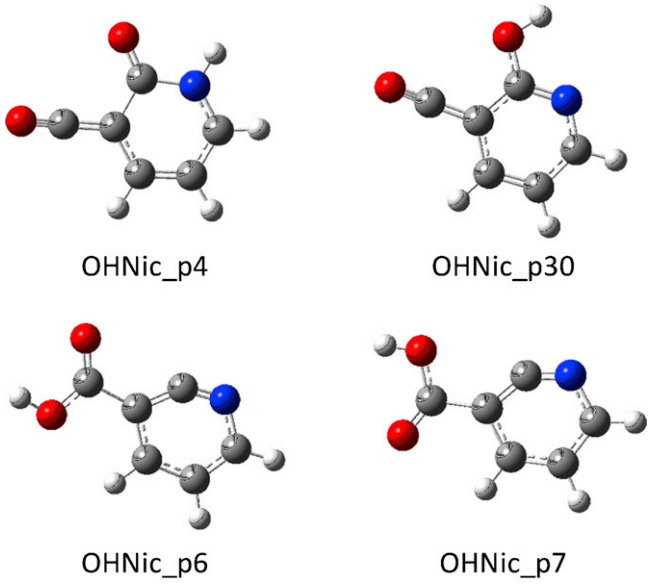

Fig. 3. Structures predicted for dehydrated product ion (*m*/*z* 122) derived from protonated 2-hydroxynicotinic acid (B3LYP/6-311+G(d,p) level of theory).

Table 1
Calculated energies for minima identified for protonated 2-hydroxynicotinic acid.

	E	ZPE	*E* + ZPE	Δ*E* (kJ/mol)
6-311+G(d,p)				
OHNic_p1	−512.6147	0.1217	−512.4931	0
OHNic_p2	−512.6084	0.1216	−512.4868	17
OHNic_p3	−512.5606	0.1162	−512.4444	128
OHNic_p5	−512.5515	0.1183	−512.4333	157
OHNic_p8	−512.6054	0.1206	−512.4848	22
OHNic_p9	−512.5929	0.1202	−512.4727	53
OHNic_p10	−512.5757	0.1204	−512.4552	99
OHNic_p11	−512.5511	0.1159	−512.4352	152
OHNic_p20	−512.5843	0.1206	−512.4637	77
OHNic_p21	−512.5679	0.1202	−512.4476	199
6-311++G(3df,3p)				
OHNic_p1	−512.6536	0.1217	−512.5319	0
OHNic_p2	−512.6458	0.1216	−512.5242	20
OHNic_p3	−512.5963	0.1162	−512.4802	136
OHNic_p5	−512.5901	0.1185	−512.4715	159
OHNic_p8	−512.6449	0.1208	−512.5240	21
OHNic_p9	−512.6340	0.1207	−512.5133	49
OHNic_p10	−512.6152	0.1205	−512.4947	98
OHNic_p11	−512.5861	0.1158	−512.4704	162
OHNic_p20	−512.6233	0.1209	−512.5024	77
OHNic_p21	−512.6083	0.1204	−512.4879	166

Table 2
Calculated energies for minima identified for the dehydration product derived from protonated 2-hydroxynicotinic acid.

	E	ZPE	*E*+ZPE	Δ*E* (kJ/mol)
6-311+G(d,p)				
OHNic_p4	−436.0855	0.0923	−435.9932	0
OHNic_p30	−436.0743	0.0916	−435.9827	28
OHNic_p6	−436.0078	0.0900	−435.9178	198
OHNic_p7	−436.0094	0.0899	−435.9194	194
6-311++G(3df,3p)				
OHNic_p4	−436.1178	0.0923	−436.0256	0
OHNic_p30	−436.1077	0.0918	−436.0160	25
OHNic_p6	−436.0411	0.0902	−435.9509	196
OHNic_p7	−436.0427	0.0901	−435.9526	192

the ring is >20 kJ/mol higher in energy. The transition state energy for tautomerization of the acylium ion is 230 kJ/mol (Table 3), consistent with the high barrier expected for the suprafacial 1–3 proton transfer. The products derived from loss of H_2O from the ring, as formed along proposed route 1, **OHNic_p6** and **OHNic_7**, are >190 kJ/mol higher in energy that **OHNic_p4**. **OHNic_p6** and **OHNic_p7** differ in the relative orientation of the acid group with respect to the carbocation site on the pyridine ring.

3.3. IRMPD spectroscopy of protonated 2-OHNic and its dehydration product

The IRMPD spectrum of 2-OHNic was collected by monitoring the yield of the dehydrated product (*m*/*z* 122) as a function of photon energy in the region 1350–1900 cm^{-1}. In Fig. 4, the IRMPD spectrum of protonated 2-OHNic (Fig. 4a) is compared to calculated spectra for structures **OHNic_p1**, **OHNic_p2**, **OHNic_p3**, **OHNic_p5** and **OHNic_p8** (Fig. 4b–e, respectively). In Fig. 5, the IRMPD spectrum of protonated 2-OHNic is compared to those for structures **OHNic_p9**, **OHNic_p10**, **OHNic_p11**, **OHNic_p20** and **OHNic_p21** (Fig. 5a–e, respectively). The theoretical vibrational spectra shown in Figs. 4 and 5 are the result of calculations at the B3LYP/6-311++G(3df,3p) level of theory. Similar comparisons made using the 6-311+G(d,p) basis set are provided in Figures S1–S3 of the supporting information.

Table 3
Calculated energies for transition state structures identified for routes 1 through 3 shown in Scheme 1.

	E	ZPE	*E*+ZPE	Δ*E* (kJ/mol)
6-311+G(d,p)				
OHNic_TSp1_p5	−512.5183	0.1148	−512.4035	235
OHNic_TSp5_p6	−512.5370	0.1174	−512.4196	193
OHNic_TSp6_p7	−436.0001	0.0898	−435.9103	382[a]
OHNic_TSp1_p2	−512.5909	0.1207	−512.4701	60
OHNic_TSp2_p3	−512.5762	0.1173	−512.4589	90
OHNic_TSp4_p30	−436.0171	0.0869	−435.9301	330[a]
OHNic_TSp1_p8	−512.6065	0.1176	−512.4889	11
OHNic_TSp8_p9	−512.5835	0.1183	−512.4652	73
OHNic_TSp9_p10	−512.5594	0.1189	−512.4405	138
OHNic_TSp10_p11	−512.5002	0.1147	−512.3855	282
6-311++G(3df,3p)				
OHNic_TSp1_p5	−512.5566	0.1149	−512.4418	237
OHNic_TSp5_p6	−512.5751	0.1176	−512.4575	195
OHNic_TSp6_p7	−436.0335	0.0899	−435.9436	383[a]
OHNic_TSp1_p2	−512.6294	0.1207	−512.5087	60
OHNic_TSp2_p3	−512.6136	0.1173	−512.4963	90
OHNic_TSp4_p30	−436.0505	0.0871	−435.9635	331[a]
OHNic_TSp1_p8	−512.6460	0.1179	−512.5281	10
OHNic_TSp8_p9	−512.6238	0.1184	−512.5053	70
OHNic_TSp9_p10	−512.5988	0.1190	−512.4798	137
OHNic_TSp10_p11	−512.5393	0.1149	−512.4244	282

[a] Denotes transition state energies for specific product ions to which the zero-point corrected energy of water product has been added for comparison.

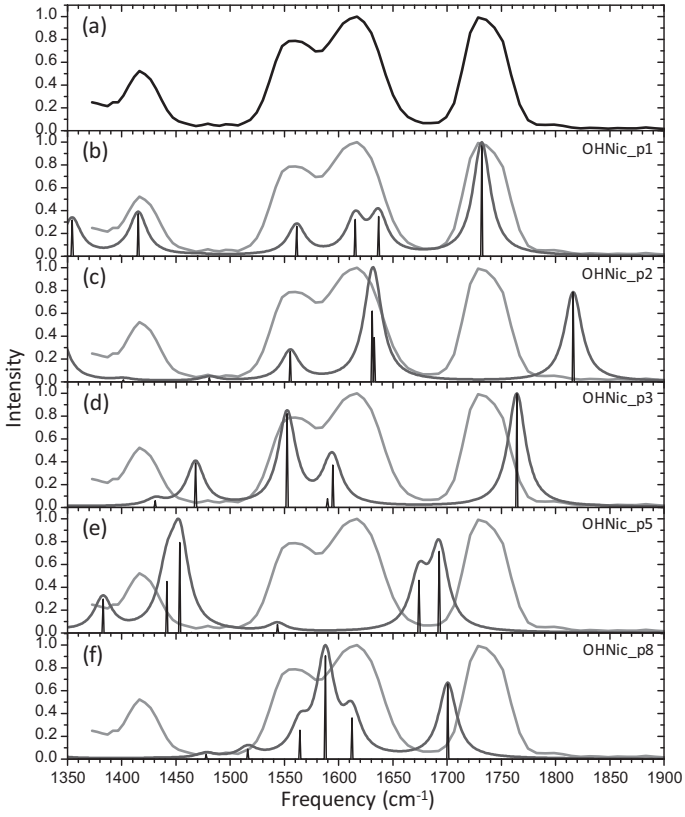

Fig. 4. IRMPD spectrum of 2-hydroxynicotinic acid (a) and predicted (B3LYP/6-311++G(3df,3p) level of theory) IR spectra for structures, (b) OHNic_p1, (c) OHNic_p2, (d) OHNic_p3, (e) OHNic_p5 and (f) OHNic_p8. The IRMPD spectrum is included as a light gray trace in (b) through (f) to facilitate comparison of experimental and theoretical results.

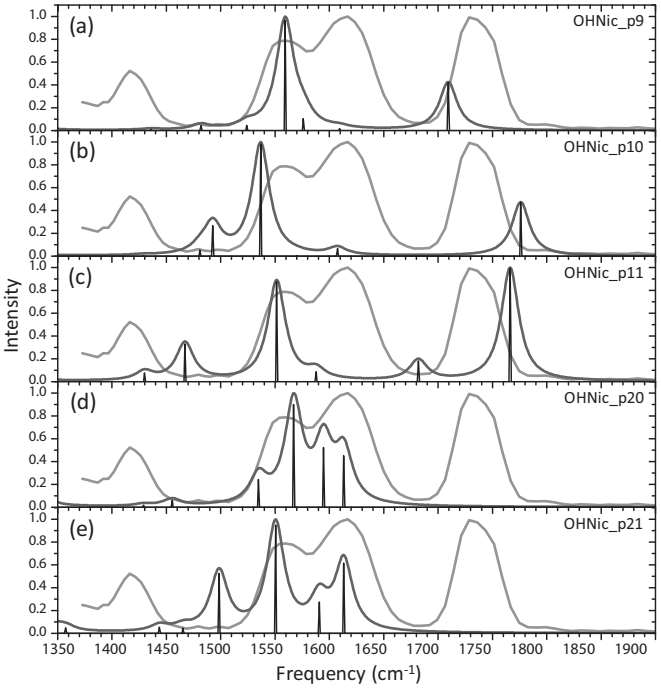

Fig. 5. Comparison of IRMPD spectrum (light gray trace) of protonated 2-hydroxynicotinc acid to spectra predicted (B3LYP/6-311++G(3df,3p) level of theory) for structures (a) OHNic_p9, (b) OHNic_p10, (c) OHNic_p11, (d) OHNic_p20 and (e) OHNic_p21.

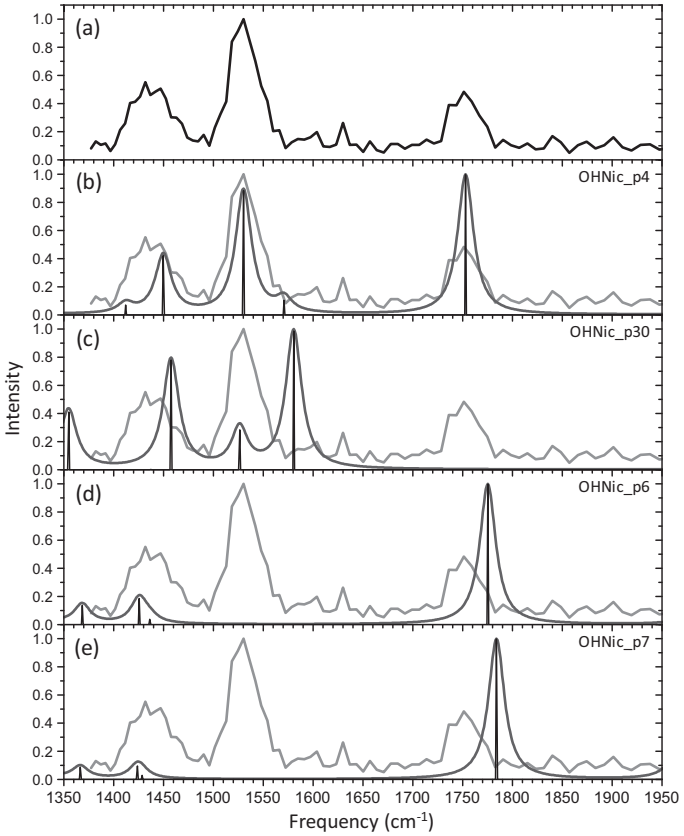

Fig. 6. IRMPD spectrum of dehydrated product ion (*m/z* 122) derived from CID of 2-hydroxynicotinic acid (a) and predicted (B3LYP/6-311++G(3df,3p) level of theory) IR spectra for structures, (b) OHNic_p4, (c) OHNic_p30, (d) OHNic_p6 and (e) OHNic_p7. The IRMPD spectrum is included as a light gray trace in (b) through (f) to facilitate comparison of experimental and theoretical results.

The IRMPD spectrum contains 4 prominent absorptions. Two absorptions at ca. 1420, and 1735 cm^{-1}, are fully resolved. Two absorptions at 1550 and 1615 cm^{-1} are less well resolved, but still clearly distinguishable. It is clear from inspection of Figs. 4 and 5 that the best agreement between experimental and theoretical spectra is for structure **OHNic_p1**, consistent with the fact that the same species is predicted to be lowest in energy. All other minima identified for protonated 2-OHNic have predicted IR features that are in poorer agreement, in terms of the relative positions of absorptions, with the experimental IRMPD spectrum.

Based on comparison to the vibrational pattern predicted for **OHNic_p1** at the B3LYP/6-311++G(3df,3p) level of theory, the absorption at 1735 cm^{-1} is assigned to the C═O stretch of the acid group coupled to C—C stretches of the protonated 2-pyridone ring. The absorption in the IRMPD spectrum located at 1615 cm^{-1} is assigned to a pair of closely spaced absorptions, predicted to appear at 1612 and 1637 cm^{-1}, that are best described as C—C stretches coupled to an —OH wag of the 2-pyridone ring. The absorptions at 1550 and 1420 cm^{-1} are assigned to different coupled modes that involve the amide N—H wag of the protonated 2-pyridone ring and ring C—C stretches.

In Fig. 6, the IRMPD spectrum of the dehydrated product (Fig. 6a) is compared to those predicted for **OHNic_p4**, **OHNic_p30**, **OHNic_p6** and **OHNic_p7** (Fig. 6b–d, respectively). The IRMPD spectrum for the dehydrated product contains 3 absorptions at ca. 1430, 1530, and 1750 cm^{-1}. The best general agreement between IRMPD and predicted spectra is for **OHNic_p4**, the 2-pyridone-like acylium ion predicted to be lowest in energy (Table 2). The key distinguishing feature of an acylium ion would be the —C≡O stretch [40,41]. For structure **OHNic_p4**, this feature is predicted to appear at ~2200 cm^{-1}, which is outside the photon energy range that could be accessed during the experiments. However, for the 2-pyridone or hydroxypyridine-type structures, absorptions characteristic of C═O stretches or N—H wags are equally telling, especially when attempting to distinguish the acylium ions from the products that resemble the nicotinic acid carbocation.

Based on the comparison to the theoretical spectrum for **OHNic_p4**, the absorption at 1750 cm^{-1} can be assigned to the C═O stretch of the ring carbonyl. The absorptions at 1530 and 1430 cm^{-1} are assigned to the N—H wag of the ring coupled to C—C stretches. For structure **OHNic_p30**, the hydroxypyridine ring tautomer of the acylium ion, the C═O stretch is predicted to red-shift by ca. 200 cm^{-1}, with the other absorptions in the region of 1530 and 1430 cm^{-1} composed only of ring C—C stretches. These absorptions are not predicted for structures **OHNic_p6** and **OHNic_p7** because the proton situated at the pyridine N atom is eliminated and the species no longer contains a ring carbonyl. The feature at 1770 and 1780 cm^{-1} in Fig. 6c and d for structures **OHNic_p6** and **OHNic_p7** correspond to the carboxylic acid C═O stretch. The small features at 1370 and 1425 cm^{-1} are best described as ring C—H wags coupled to ring C—C stretches. Clearly, based on the excellent agreement between the predicted spectrum for **OHNic_p4** and the IRMPD spectrum for the ion at *m/z* 122, the structure of the dehydrated product can be assigned to the acylium species with 2-pyridine like structure.

3.4. Pathway for loss of H_2O from protonated 2-OHNic

With the conformations of protonated 2-OHNic (*m/z* 140) and the dehydrated product ion (*m/z* 122) confidently assigned to **OHNic_p1** and **OHNic_p4**, respectively, the CID reaction that leads to elimination of H_2O can be said to generate an acylium ion. To further investigate the fragmentation pathways, DFT calculations were used to probe the reaction energies for the pathways shown in Scheme 1. The relative energies of relevant minima are provided in Tables 1 and 2. Energies for transition state structures at the B3LYP/6-311+G(d,p) and B3LYP/6-311++G(3df,3p) level of theory are provided in Table 3. Structures of the transition states for the three pathways are provided in Figs. 7–9.

Plots of relative energy versus reaction progress are provided in Figures S4–6 in the supporting information for pathways 1, 2 and 3, respectively. For pathway 1, structure **OHNic_p5** is generated from the global minimum, **OHNic_p1**, by proton transfer through transition state **OHNic_TSp1_p5**. As noted earlier, the transfer proceeds through an energetically unfavorable suprafacial 1–3 transition state. Cleavage of the ring C—OH_2 bond that ultimately causes elimination of H_2O, occurs through transition state **OHNic_TSp5_p6**, presumably furnishes structure **OHNic_p6**, the nicotinic acid carbocation. The products (**OHNic_p6** and H_2O) are ca. 362 kJ/mol above the energy of the global minimum. Rotation of the acid group, through transition state **OHNic_TSp6_7**, furnishes the lower energy structure **OHNic_p7** (ca. 358 kJ/mol).

For pathway 2 (Fig. 8), structure **OHNic_2** is populated by rotation of the acid group through transition state **OHNic_TS_p1_p2**, with a barrier of about 60 kJ/mol. Elimination of H_2O in this pathway proceeds through a 6-membered ring transition state that involves concerted proton transfer and C—OH_2 bond cleavage (structure **OHNic_TSp2_p3**) that is about 90 kJ/mol above structure **OHNic_p1**. Following elimination of H_2O, the post reaction complex **OHNic_p3** can presumably be formed. Elimination of H_2O from the post-reaction complex then furnishes the acylium ion. The rate determining step in this pathway is formation of products, which lie ca. 164 kJ/mol above the global minimum.

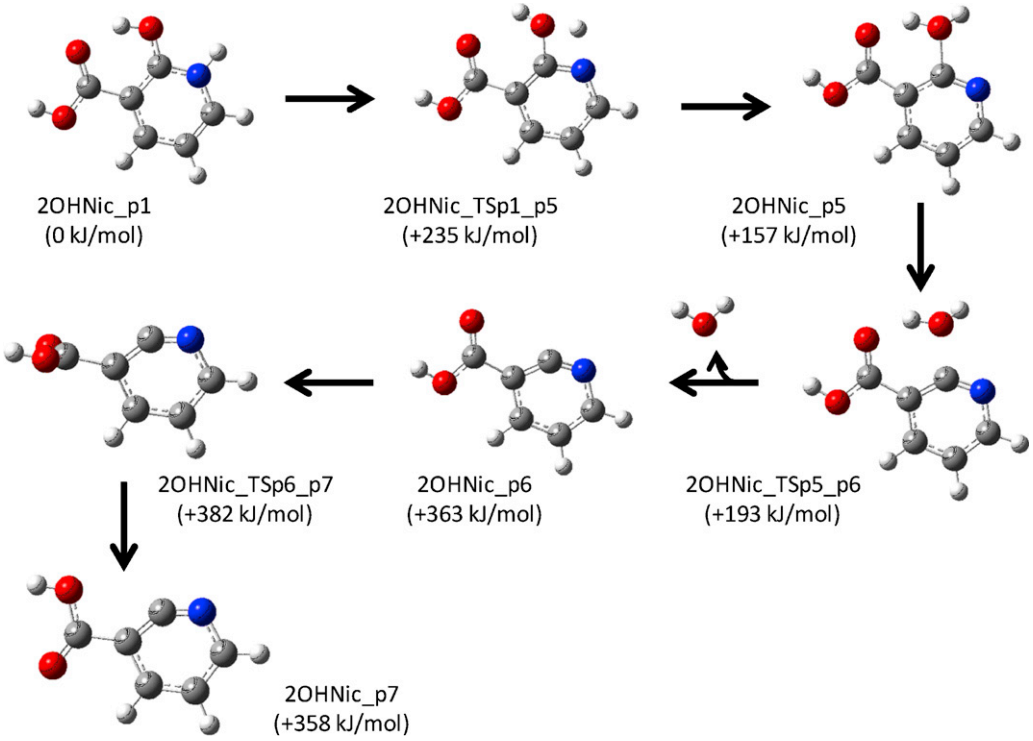

Fig. 7. Reaction pathway for generation of dehydrated product ion (*m*/*z* 122) by route 1 in Scheme 1. Relative energies for relevant species are provided in Tables 1–3 of the text.

For pathway 3 (Fig. 9), structure **OHNic_p8** is generated from the global minimum, **OHNic_p1**, by proton transfer through transition state **OHNic_TSp1_p8**. Structure **OHNic_p9** is generated from **OHNic_p8** through rotation of the acid —OH group through transition state **OHNic_TSp8_p9**. Progress through transition state **OHNic_TS_p9_p10** furnished structure **OHNic_p10**, a gem-diol conformation which allows for proton transfer (transition state structure **OHNic_TSp10_p11**) with concerted C—O bond cleavage to result in elimination of H_2O and formation of the acylium ion, **OHNic_p4**. The barrier to this reaction pathway is the suprafacial 1–3 proton transfer transition state **OHNic_TSp10_p11** that ultimately leads to elimination of H_2O, which is ~282 kJ/mol above the global minimum when calculated at either level of theory.

Based on the energetics produced by DFT, it can reasonably be assumed that loss of H_2O from protonated 2-OHNic occurs by route 2 depicted in Scheme 1. The path leads to the correct product ion as identified by IRMPD spectroscopy. The overall reaction barrier appears to be formation of products, at ~164 kJ/mol, which is significantly lower than the proton transfer barriers identified for routes 1 and 3. As noted earlier, the product ion generated by route 1 is a nicotinic acid carbocation, for which no evidence was observed in the IRMPD spectrum.

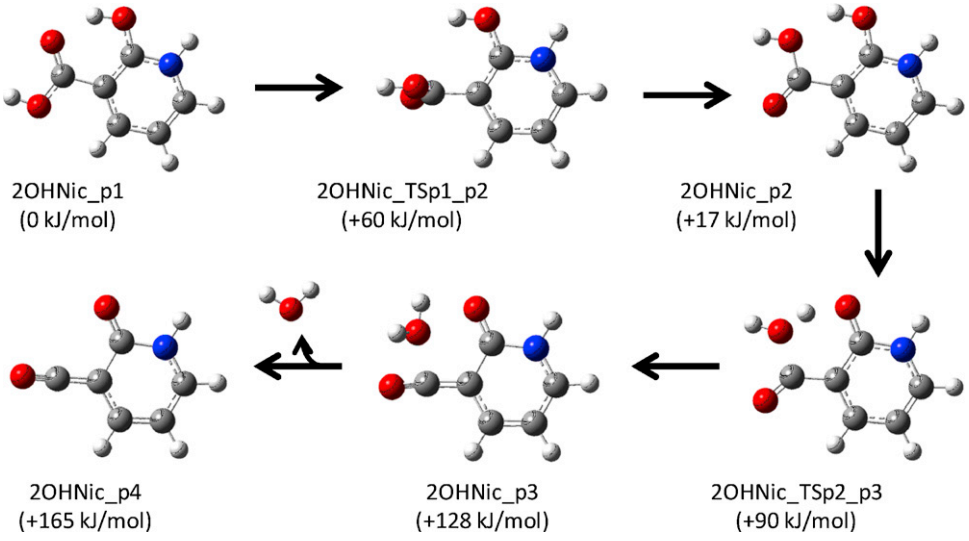

Fig. 8. Reaction pathway for generation of dehydrated product ion (*m*/*z* 122) by route 2 in Scheme 1. Relative energies for relevant species are provided in Tables 1–3 of the text.

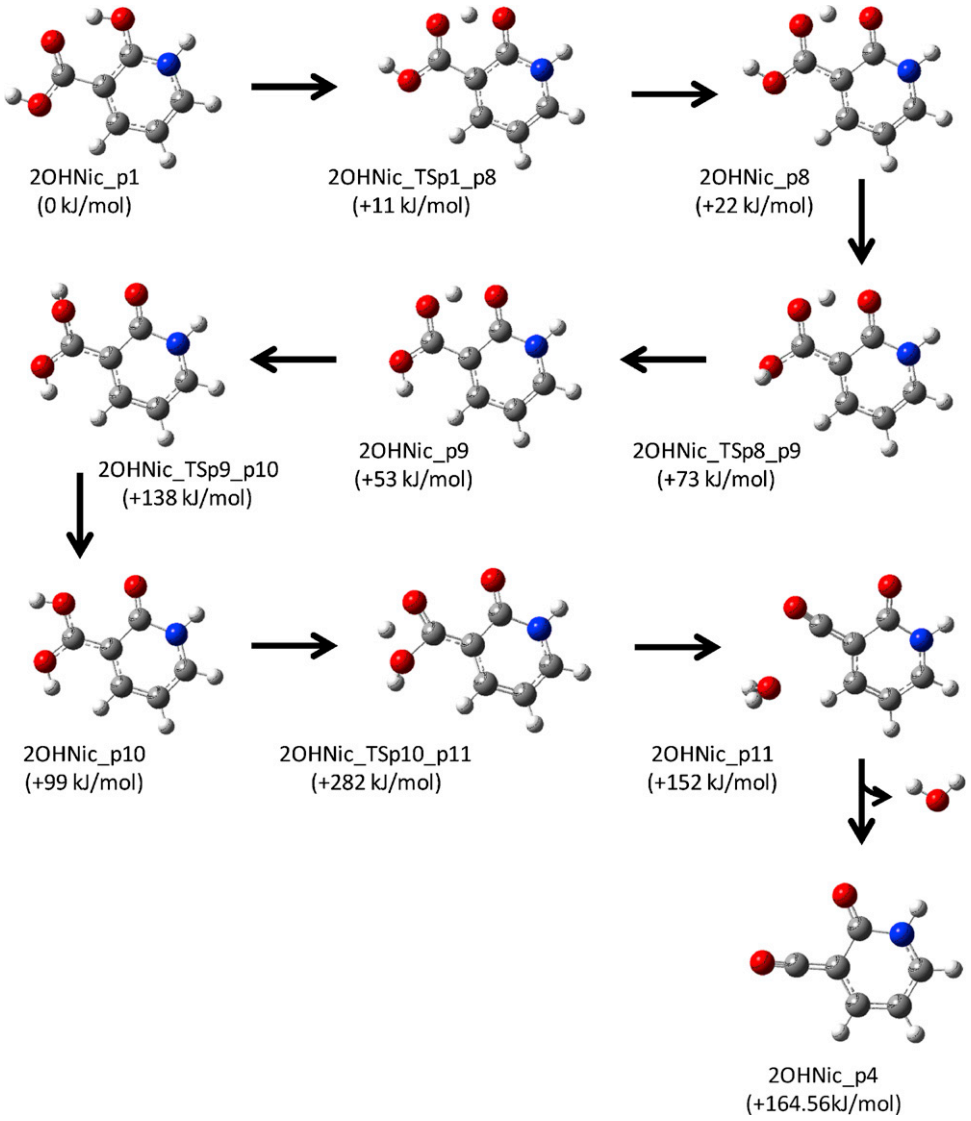

Fig. 9. Reaction pathway for generation of dehydrated product ion (m/z 122) by route 3 in Scheme 1. Relative energies for relevant species are provided in Tables 1–3 of the text.

4. Conclusions

In summary, we have shown that CID of protonated 2-hydroxynicotinic acid (2-OHNic) generates a dominant product ion through the elimination of water, which subsequently forms an adduct with adventitious H_2O in a quadrupole ion trap in an ion-molecule reaction. The formation of the adduct species was confirmed by isolating and storing the product in the ion trap mass spectrometer, without imposed collisional activation. Adduct formation is identified by new peaks 18 and 32 mass units higher and presumably represents generation of acid and methyl ester species by reaction of an acylium ion with water and methanol.

Density functional theory calculations indicate that an acylium ion is energetically more favored as the dehydration product from 2-OHNic than a nicotinic acid carbocation generated by elimination of H_2O from the aromatic ring. Formation of the acylium product is confirmed by IRMPD spectroscopy following comparison to harmonic calculations by DFT. The IR spectrum of the dehydration product is most consistent with formation of an acylium ion with a 2-pyridone-like structure rather than the hydroxypyridine tautomer.

DFT was also used to investigate in detail the dynamics of possible reaction pathways to the dehydrated product. Investigation of three possible routes to loss of H_2O from protonated 2-OHNic demonstrates that the lowest energy pathway leads to an acylium ion by concerted proton transfer and elimination of H_2O through a 6-membered ring transition state. The other pathways include energetically unfavorable 1–3 proton transfer steps and, in one case, the formation of an energetically unfavorable product ion.

Acknowledgements

Funds to purchase the LCQDeca mass spectrometer were provided by Wichita State University and the State of Kansas NSF EPSCoR program. JO and GB are supported by the Nederlandse Organisatie voor Wetenschappelijk Onderzoek (NWO). Construction and shipping of the FT-ICR-MS instrument was made possible through funding from the National High Field FT-ICR Facility (grant CHE-9909502) at the National High Magnetic Field Laboratory, Tallahassee, FL. The excellent support by Dr. B. Redlich and others of the FELIX staff is gratefully acknowledged.

Appendix A. Supplementary data

Supplementary data associated with this article can be found, in the online version, at http://dx.doi.org/10.1016/j.ijms.2012.06.026.

References

[1] A.R. Dongre, J.L. Jones, A. Somogyi, V.H. Wysocki, Journal of the American Chemical Society 118 (1996) 8365–8374.
[2] V.H. Wysocki, G. Tsaprailis, L.L. Smith, L.A. Breci, Journal of Mass Spectrometry 35 (2000) 1399–1406.
[3] D.F. Hunt, J.R. Yates III, J. Shabanonowitz, S. Winston, C.R. Hauer, Proceedings of the National Academy of Sciences 83 (1986) 6233–6237.
[4] K. Biemann, Biomedical and Environmental Mass Spectrometry 16 (1988) 99–111.
[5] H. Steen, M. Mann, Nature Reviews Molecular Cell Biology 5 (2004) 699–711.
[6] T. Yalcin, I.G. Csizmadia, M.B. Peterson, A. Harrison, Journal of the American Society for Mass Spectrometry 7 (1996) 233–242.
[7] B. Paizs, G. Lendvay, K. Vekey, S. Suhai, Rapid Communications in Mass Spectrometry 13 (1999) 525–533.
[8] B. Paizs, S. Suhai, Journal of the American Society for Mass Spectrometry 15 (2004) 103–113.
[9] B. Paizs, S. Suhai, Rapid Communications in Mass Spectrometry 16 (2002) 375–389.
[10] M.J. Polce, D. Ren, C. Wesdemiotis, Journal of Mass Spectrometry 35 (2000) 1391–1398.
[11] B. Paizs, S. Suhai, Mass Spectrometry Reviews 24 (2004) 508–548.
[12] S. Molesworth, C.M. Leavitt, G.S. Groenewold, J. Oomens, J. Steill, M. van Stipdonk, Journal of the American Society for Mass Spectrometry 20 (2009) 1841–1845.
[13] M.J. Van Stipdonk, D.R. Kerstetter, C.M. Leavitt, G.S. Groenewold, J.D. Steill, J. Oomens, Physical Chemistry Chemical Physics 10 (2008) 3209–3221.
[14] G.A. Olah, P.v.R. Schleyer (Eds.), Carbonium Ions, vol. V, John Wiley and Sons Inc., New York, 1976, p. 295.
[15] D. Bethell, V. Gold, Carbonium Ions: An Introduction, Academic Press Inc., New York, 1967, p. 285.
[16] B.D. Song, W.P. Jencks, Journal of the American Chemical Society 111 (1989) 8470–8479.
[17] R.A. Cox, K. Yates, Canadian Journal of Chemistry 60 (1982) 3061–3070.
[18] R.A. Cox, Canadian Journal of Chemistry 86 (2008) 290–297.
[19] R.W. Boyd, R. Morrison, Robert, Organic Chemistry, Prentice Hall, Englewood Cliffs, NJ, 1992, pp. 666–762.
[20] T. Laue, A. Plagens, Named Organic Reactions, 2nd edition, John Wiley & Sons, New York, 2005, p. 320.
[21] M. Hayashi, Journal of the Chemical Society (1927) 2516–2527.
[22] R.B. Sandin, R. Melby, R. Crawford, D. McGreer, Journal of the American Chemical Society (1956) 3817–3819.
[23] G.S. Groenewold, J. Oomens, W.A. de Jong, G.L. Gresham, M.E. McIlwain, M.J. Van Stipdonk, Physical Chemistry Chemical Physics 10 (2008) 1192.
[24] G.S. Groenewold, A.K. Gianotto, K.C. Cossel, M.J. Van Stipdonk, D.T. Moore, N. Polfer, J. Oomens, W.A. de Jong, L. Visscher, Journal of the American Chemical Society 107 (2006) 4802.
[25] G.S. Groenewold, A.K. Gianotto, K.C. Cossel, M.J. Van Stipdonk, J. Oomens, N. Polfer, D.T. Moore, W.A. de Jong, M.E. McIlwain, Physical Chemistry Chemical Physics 9 (2006) 596.
[26] G.S. Groenewold, A.K. Gianotto, M.E. McIlwain, M.J. Van Stipdonk, M. Kullman, D.T. Moore, N. Polfer, J. Oomens, I. Infante, L. Visscher, B. Siboulet, W.A. de Jong, Journal of Physical Chemistry A 112 (2008) 508.
[27] G.S. Groenewold, M.J. Van Stipdonk, W.A. de Jong, J. Oomens, G.L. Gresham, M.E. McIlwain, D. Gao, B. Siboulet, L. Visscher, M. Kullman, N. Polfer, Physical Chemistry Chemical Physics 9 (2008) 1278.
[28] J.J. Valle, J.R. Eyler, J. Oomens, D.T. Moore, A.F.G. van der Meer, G. von Helden, G. Meijer, C.L. Hendrickson, A.G. Marshall, G.T. Blakney, Review of Scientific Instruments 76 (2005) 023103.
[29] V.N. Bagratashvili, V.S. Letokov, A.A. Makarov, E.A. Ryabov, Multiple Photon Infrared Laser Photophysics and Photochemistry, Harwood, Chur, Switzerland, 1985.
[30] D.T. Moore, J. Oomens, J.R. Eyler, G. von Helden, G. Meijer, R.C. Dunbar, Journal of the American Chemical Society 127 (2005) 7243.
[31] J. Oomens, A.G.G.M. Tielens, B.G. Sartakov, G. von Helden, G. Meijer, Astrophysics Journal 591 (2003) 968.
[32] M.J. Frisch, G.W. Trucks, H.B. Schlegel, G.E. Scuseria, M.A. Robb, J.R. Cheeseman, J.A. Montgomery Jr., T. Vreven, K.N. Kudin, J.C. Burant, J.M. Millam, S.S. Iyengar, J. Tomasi, V. Barone, B. Mennucci, M. Cossi, G. Scalmani, N. Rega, G.A. Petersson, H. Nakatsuji, M. Hada, M. Ehara, K. Toyota, R. Fukuda, J. Hasegawa, M. Ishida, T. Nakajima, Y. Honda, O. Kitao, H. Nakai, M. Klene, X. Li, J.E. Knox, H.P. Hratchian, J.B. Cross, V. Bakken, C. Adamo, J. Jaramillo, R. Gomperts, R.E. Stratmann, O. Yazyev, A.J. Austin, R. Cammi, C. Pomelli, J.W. Ochterski, P.Y. Ayala, K. Morokuma, G.A. Voth, P. Salvador, J.J. Dannenberg, V.G. Zakrzewski, S. Dapprich, A.D. Daniels, M.C. Strain, O. Farkas, D.K. Malick, A.D. Rabuck, K. Raghavachari, J.B. Foresman, J.V. Ortiz, Q. Cui, A.G. Baboul, S. Clifford, J. Cioslowski, B.B. Stefanov, G. Liu, A. Liashenko, P. Piskorz, I. Komaromi, R.L. Martin, D.J. Fox, T. Keith, M.A. Al-Laham, C.Y. Peng, A. Nanayakkara, M. Challacombe, P.M.W. Gill, B. Johnson, W. Chen, M.W. Wong, C. Gonzalez, J.A. Pople, Gaussian 03, Revision D.01, Gaussian, Inc., Wallingford, CT, 2004.
[33] S. Catinella, N. Pelizzi, S. Barboso, D. Favretto, R. Seraglia, P. Traldi, Rapid Communications in Mass Spectrometry 16 (2002) 1897–1902.
[34] D. Goeringer, D.C. Duckworth, S.A. McLuckey, Journal of Physical Chemistry A 105 (2001) 1882–1889.
[35] G.L. Gresham, A.K. Gianotto, P.B. Harrington, L. Cao, J.R. Scott, J.E. Olson, A.D. Appelhans, M.J. Van Stipdonk, G.S. Groenewold, Journal of Physical Chemistry A 107 (2003) 8530–8538.
[36] W. Chien, D. Hanna, V. Anbalagan, G. Gresham, G. Groenewold, M. Zandler, M.J. Van Stipdonk, Journal of the American Society for Mass Spectrometry 15 (2004) 777–783.
[37] Z. Guan, J.M. Liesch, Journal of Mass Spectrometry 36 (2001) 264–276.
[38] P. Neta, B. Godugu, Y. Liang, Y. Simón-Manso, X. Yang, S. Stein, Rapid Communications in Mass Spectrometry 24 (2010) 3271–3278.
[39] A. Kaufmann, P. Butcher, K. Maden, M. Widmer, K. Giles, D. Uria, Rapid Communications in Mass Spectrometry 23 (2009) 985–998.
[40] J. Oomens, J.M. Bakker, B.G. Sartakov, G. Meijer, G. von Helden, Chemical Physics Letters 367 (2003) 576–580.
[41] J. Oomens, D.T. Moore, G. Meijer, G. von Helden, Physical Chemistry Chemical Physics 6 (2004) 710–718.